Hydrodynamic theory for spatially inhomogeneous semiconductor lasers. II. Numerical results

Jianzhong Li* and C. Z. Ning†
Computational Quantum Optoelectronics, NASA Ames Research Center, Mail Stop N229-1, Moffett Field, California 94035-1000
(Received 31 December 2001; published 6 August 2002)

We present numerical results for the diffusion coefficients (DCs) in the *coupled diffusion model* derived [J. Li and C. Z. Ning, preceding paper, Phys. Rev. A **66**, 023802 (2002)] for a semiconductor quantum well. These include self- and mutual-diffusion coefficients in the general two-component case, as well as density- and temperature-related DCs under the single-component approximation. The results are analyzed from the viewpoint of the free Fermi gas theory with many-body effects incorporated. We discuss in detail the dependence of these DCs on densities and temperatures in order to identify different roles played by the free-carrier contributions including carrier statistics and carrier–LO-phonon scattering, and many-body corrections including band-gap renormalization and electron-hole (e-h) scattering. In the general two-component case, it is found that the self- and mutual-diffusion coefficients are determined mainly by the free-carrier contributions, but with significant many-body corrections near the transition density where carrier statistics changes from the Maxwell to the Fermi-Dirac distribution. Carrier–LO-phonon scattering is dominant at low density, whereas e-h scattering becomes important in determining their density dependence above the electron transition density. In the single-component case, it is found that many-body effects decrease the density coefficients but enhance the temperature coefficients. The modification is on the order of 10% and reaches a maximum of over 20% [C. Z. Ning and J. Li, Phys. Rev. B **65**, 201305(R) (2002)] for the density coefficients. Overall, temperature elevation enhances the diffusive capability of carriers (DCs) linearly, and such an enhancement grows with density. The complete data set of various DCs as functions of carrier densities and temperatures provides necessary ingredients for future applications of the *model* to various spatially inhomogeneous optoelectronic devices.

DOI: 10.1103/PhysRevA.66.023803 PACS number(s): 42.55.Px, 42.65.Sf, 78.20.Bh

I. INTRODUCTION

In the preceding theoretical paper [1], we have derived a set of *coupled diffusion equations* for the densities and temperatures of electrons and holes in a spatially inhomogeneous semiconductor quantum well (QW). Our derivation is based on a microscopic kinetic theory for the electron-hole plasma (EHP) model. Such a first-principles approach allows us to derive explicit expressions for all momentum and energy (thus temperature) relaxation rates, and for various diffusion coefficients (DCs) in the general two-component (TC) case and the single-component (SC) case. The SC case is treated within the standard ambipolar diffusion approximation or in strong electron-hole (e-h) scattering limit. The DCs are given in terms of momentum relaxation rates, many-body corrections, and the derivatives of carrier thermal energies [1]. Ultimately, the coefficients become functions of the thermodynamic variables of the EHP through these quantities. The application of the model is not restricted to lasing devices. Rather, it can be easily adapted for EHPs in other types of devices, such as photodetectors and photoconducting devices. Obviously, applications of this *coupled diffusion model* (CDM) rely upon the knowledge of those related diffusion coefficients.

The purpose of the present paper is twofold: First, we want to analyze in detail the behaviors of these DCs and understand them in terms of the underlying physics processes. As we will show, all features of the DCs can be explained in terms of the Fermi gas theory with corrections from many-body effects [2]. Second, we want to present a complete data set for these DCs as functions of densities and temperatures to provide guidance for any future applications of the CDM to various optoelectronic devices. Since most of such applications will involve extensive simulations of the partial differential equations, it is essential to have those DCs tabulated and eventually fitted as analytical functions of densities and temperatures beforehand so that time-consuming microscopic calculations do not have to be repeated.

For the numerical results, we choose an 8-nm $Al_{0.3}Ga_{0.7}As/GaAs$ quantum well structure as the model material system. Relevant material parameters are well documented in the literature, but listed here for completeness. For this structure, typical plasma density is 10^{12} cm^{-2} for room-temperature lasing operations. Thus, the ranges for the thermodynamic variables are chosen for densities from 10^{10} to 10^{13} cm^{-2} and for temperatures from 200 to 400 K. To manage the already very lengthy analysis, we shall not further differentiate temperatures between electrons and holes and shall use the term ''plasma temperature'' to denote the common temperature. As shown in the numerical results, temperature plays a very predictable role. Additionally, we restrict our presentation and discussions to density-related results at 300 K only for the general TC case and discuss the temperature-related coefficients only for the SC case.

To help the discussions in the two-component case, we distinguish carrier types (electrons and holes) and their associated variables as primary and secondary ones when diffusion coefficients are presented. Such an assignment stems from the fact that a coefficient relates the gradient of one

*Electronic address: jianzhng@nas.nasa.gov
†Electronic address: cning@mail.arc.nasa.gov; URL: http://www.nas.nasa.gov/~cning

(called) primary variable to the current of another (called) secondary variable [cf. Eq. (C1) in Ref. [1]]. For example, for the diffusion coefficient $D_{N^\alpha N^\beta}$, where $\alpha,\ \beta \in \{e,h\}$, we refer to N^β as the primary carrier density, or simply primary density, and the β carriers as primary carriers. Accordingly, N^α is referred to as the secondary carrier density, or simply secondary density, and the α carriers as secondary carriers. As an extension to this convention, the primary type is the same as the secondary one for a quantity with only one carrier type in its index, even though the quantity may depend on variables of the other type implicitly. The coefficient $D_{N^\alpha N^\alpha}$ and factor μ_α are such instances, which are functions of not only the primary density N^α and temperature T^α, but also the secondary density N^β and temperature T^β. Finally, in order to be consistent with this convention, for all other quantities or terms denoted by both carrier types, their primary type follows their associated DCs. For instance, for the term $H^e_{N^h}$, which appears in Eq. (6), its primary carrier type is the holes.

The paper is organized as follows. In Sec. II, we summarize those key results in two-dimensional (2D) Fermi gas theory which are critical in understanding the diffusion coefficients. Then, we present and discuss the carrier momentum and temperature relaxation rates due to carrier–LO-(longitudinal-optical) phonon scattering and electron-hole (e-h) scattering in Sec. III. Density diffusion coefficients in the general two-component case are presented and analyzed in Sec. IV, followed by all the DCs for the two-component case in Sec. V. A summary is given in Sec. VI for the numerical results, together with concluding remarks regarding the scope and validity of the CDM, many-body effects, and a comparison with 3D results in the literature.

II. KEY RESULTS OF 2D FERMI GAS THEORY

Since properties of the ideal Fermi gas will be important in understanding the behavior of the momentum relaxation rates and all the DCs, we summarize certain key results of the 2D Fermi gas theory. These results are obtained by applying the independent electron approximation [3]. Furthermore, some terms frequently referred to in this paper shall be introduced in this section.

First of all, the carrier thermal energies W^α's of the 2D EHP can be approximated [cf. Eq. (D8) in Ref. [1]] as follows:

$$W^\alpha = \begin{cases} N^\alpha k_B T^\alpha, & \text{classical limit,} \\ w_0^\alpha N^{\alpha 2} + w_2^\alpha T^{\alpha 2}, & \text{degenerate limit,} \end{cases} \tag{1}$$

where we have indicated the statistics applicable in each case. Within the limited temperature range between 200 K and 400 K considered in this paper, the statistical property or the degeneracy is determined by the density alone. While the first line of Eq. (1) is the familiar classical result of the Boltzmann statistics, the second line is obtained for the degenerate limit using the Sommerfeld expansion. The first term has a quadratic density dependence, but no temperature dependence. The remaining term contributes to all the temperature dependence. Summarily, the free-carrier thermal energy has a bilinear combination of density and temperature in the classical regime, while it is the sum of two quadratic terms of temperature and density. Thus, it follows naturally that the density (temperature) derivative is independent of density (temperature), while being linearly dependent on temperature (density) in the classical regime. However, in the degenerate limit, the density (temperature) derivative depends linearly on density (temperature), while having no dependence on temperature (density). Obviously, the energy derivatives (or specific heats) in the two limits exhibit different behaviors. Since the DCs are closely related to such derivatives, we expect different behaviors of DCs in the two limits. The physical origin of the different behaviors is due to statistical degeneracy or Pauli's principle in the quantum regime. In the interested density and temperature domain of this study, carrier behaviors are somewhere between the two limits.

Next, we illustrate how the transition from the classical regime to the quantum regime can be quantitatively characterized and what role different masses of electrons and holes play. It can be shown [see Eq. (D10) and related expressions in Ref. [1]] that the density derivative of the thermal energy of α carriers is given by

$$\partial_{N^\alpha} W^\alpha = \frac{\pi \hbar^2 N^\alpha}{m_\alpha}\left[1 + \exp\left(-\frac{\mu_F^\alpha}{k_B T^\alpha}\right)\right], \tag{2}$$

where μ_F^α is the chemical potential of α carriers. The chemical potential for fermionic particles increases monotonically with their density owing to Pauli's principle. To be exact, the chemical potential depends linearly on the density in the degenerate limit. In the classical limit, however, $\partial_{N^\alpha} W^\alpha = k_B T^\alpha$ as the exponential term above becomes important as the chemical potential gets negatively large. Therefore, it is clearly shown by the preceding equation that the carrier density corresponding to zero chemical potential is an excellent quantitative indicator for the transition from the classical regime to the quantum regime. Such a density is called ''the critical density'' in some literature [4], even though nothing critical occurs of statistical nature at this density. In this paper, we use the term ''transition density'' instead to denote this transition. This 2D transition density is given by

$$n_{t,\alpha}^{2\mathrm{D}} = \frac{m_\alpha k_B T}{\pi \hbar^2} \ln 2, \tag{3}$$

which is about 5×10^{11} cm^{-2} for electrons and 3×10^{12} cm^{-2} for holes at room temperature. As defined, the transition density provides a quantitative measure above which statistical degeneracy for fermionic particles becomes important. As a consequence of statistical degeneracy, phase-space-filling effects greatly influence the physical properties of the Fermi gas in the quantum regime ($N^\alpha > n_{t,\alpha}^{2\mathrm{D}}$). In this regime, energy for the 2D Fermi gas is on the order of the chemical potential, instead of the thermal energy $k_B T$ in the classical regime ($N^\alpha < n_{t,\alpha}^{2\mathrm{D}}$). The constant density of states in 2D leads to the linear relationship between chemical potential and density, as mentioned earlier. Therefore, this change

TABLE I. Parameters and their values. All values are from Ref. [19] except where indicated otherwise.

m_e	Effective electron mass[a]	$0.067m_0$	m_h	Effective hole mass	$0.45m_0$
ε_s	Static permittivity	13.1	ε_∞	High-frequency permittivity	10.9
$\hbar\omega_{\mathrm{LO}}$	LO-phonon energy	35.0 meV	C[b]		4

[a]In units of free-electron mass.
[b]A numerical constant used in the single-plasmon-pole model for screening (see Ref. [6]).

in energy scale results in corresponding behavioral transitions in the physical properties of the Fermi gas, as a manifestation of phase-space-filling effects. Such transitions start near the transition density.

Now let us discuss the case of an EHP. The total thermal energy of the plasma is the sum of that of electrons and holes. Because of their different masses, the lighter electrons step into the quantum regime before the holes do ($n_{t,e}^{2\mathrm{D}} < n_{t,h}^{2\mathrm{D}}$). After the transition for electrons, their contribution to the total thermal energy becomes larger than holes, as a result of the stronger density dependence. Therefore, the transitional behavior of electrons masks that of holes, as far as density derivatives of the thermal energies are concerned. However, the story is not complete without considering temperature derivatives of the thermal energies. It is interesting to show [see Eqs. (D10) and (D11) in Ref. [1]] that the following relationship holds for any density and temperature:

$$N^\alpha \partial_{N^\alpha} W^\alpha + T^\alpha \partial_{T^\alpha} W^\alpha = 2W^\alpha. \tag{4}$$

This is in fact Euler's theorem for homogeneous functions of degree 2, which states that the thermal energy is a linear superposition of quadratic polynomials in density and temperature. This equation dictates that both w_0^α and w_2^α are independent of density and temperature in the degenerate limit, being consistent with, and as indicated by, Eq. (1). However, the first term dominates over the second term quantitatively, which is what the above equation fails to reveal and why electronic specific heat is much smaller in a normal metal than in an ideal gas. As such, we see immediately that the hole transition density masks the electron transition density for temperature derivatives. Nevertheless, it is important to point out that around the transition density continuous behaviors are anticipated. As the upper density bound studied in this paper is marginally higher than the hole transition density, we expect deviations of the system behavior from that of the limiting cases. One such deviation is the density dependence of the temperature derivatives that does exist above the transition density, but this dependence weakens as density increases. Finally, it is also true that for many physical quantities of the EHP, neither the electron transition density nor the hole transition density properly characterizes the statistical transition, because the EHP is a mixture of electrons and holes after all. Instead, the transparency density of the EHP, given by $\mu_F^e + \mu_F^h = 0$ and denoted by $n_{tr}^{2\mathrm{D}}$, is a better indicator of the transition, especially for neutral plasmas. The density has a magnitude between the electron transition density and the hole transition density. This can be easily seen from its definition, since the chemical potential is a monotonic function of density. In most cases in this paper, the transition density of the predominant carrier type is the appropriate one for characterization of the statistical transition; otherwise, the transparency density is a better choice.

To close this section, we emphasize that the transition densities introduced here are useful for a general understanding of the numerical results presented in this paper, as their existence is a revelation of the fermionic nature of the EHP. They will be extensively referred to later as we discuss the underlying physics of the numerical results.

III. MOMENTUM AND TEMPERATURE RELAXATION RATES

Momentum relaxation is the underlying physics process for carrier diffusion, and various momentum relaxation rates appear naturally in the expression of DCs as we will see in the following section. To prepare ourselves for the explanation of the diffusion coefficients, we present in this section the relaxation rates obtained microscopically (cf. Appendix B in Ref. [1]). In short, the rates are treated within the second Born approximation [5]. Screening of the Coulomb interaction is described under the single-plasmon-pole model [6,7]. Numerical integration for the rates is implemented with 40-point Gaussian quadratures after necessary simplifications. Both momentum and temperature relaxation rates are shown, but only the momentum relaxation rates affect the DCs. The temperature relaxation (or the Newton's cooling) rates are used in the temperature equation(s) in the CDM. Two major scattering mechanisms are considered in the EHP model: *e-h* and carrier–LO-phonon (c-LO) scatterings. Table I contains parameters and their numerical values used in our calculations.

Results for momentum relaxation rates due to *e-h* [Eq. (A10) in Ref. [1]] and c–LO-phonon [Eq. (B6) in Ref. [1]] scattering are presented in Fig. 1. For the *e-h* scattering rates shown, equal electron and hole densities are chosen. At low density, the *e-h* scattering rate shows a linear density dependence, while the c-LO scattering rates are density independent. All the rates decrease above a certain transition density which increases with temperature. The transition density is higher for holes than for electrons. For the *e-h* scattering rate, the decrease starts along with the e-LO scattering rates. Overall, temperature dependence is relatively weak for all the rates. Specifically, a temperature rise leads to a decrease of all the rates at low density, but to an increase above the transition density. Our quantitative comparison shows that this transition density is nothing but the density $n_{t,\alpha}^{2\mathrm{D}}$ defined earlier in Eq. (3). Furthermore, the temperature and carrier-type dependences of this transition density agree well with those of the density $n_{t,\alpha}^{2\mathrm{D}}$. Thus, this characteristic change for

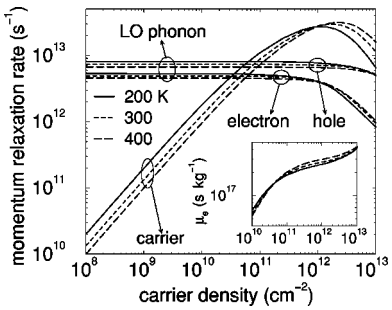

FIG. 1. Carrier momentum relaxation rates as a function of density and temperature. All the results shown in this paper are for an 8-nm $Al_{0.3}Ga_{0.7}As/GaAs$ quantum well. The inset shows the μ_e factor given by Eq. (34) in Ref. [1]. The electron density and hole density are identical for the electron-hole scattering and the μ_e factor here. Note that this μ_e factor is different from that used under the single-component approximation [cf. Eq. (13)] and is not carrier mobility either.

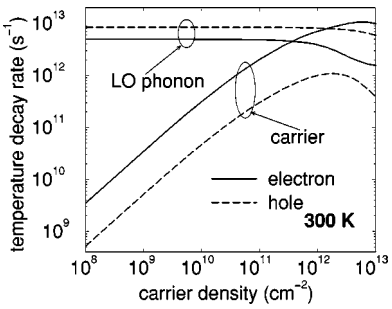

FIG. 2. Comparison of carrier temperature relaxation rates as a function of density and temperature. The results shown are obtained microscopically following Appendixes A and B in Ref. [1].

the rates across the transition density is associated with change from classical to quantum statistics of the fermionic particles, which is explained in detail next.

At low density, carriers follow the Maxwell distribution and behave independently. Thus, the c–LO-phonon scattering rates are density independent. The *e-h* scattering rate, because of its binary nature, is directly proportional to the secondary density (type β), and is independent of the primary density (type α). As the two densities are the same in Fig. 1, we see the linear density dependence. In contrast, in the quantum regime phase-space-filling effects become important owing to Pauli's principle. Limitation to the available phase space for carrier scattering causes reduction in the scattering rates. Both carrier types are subject to the phase-space-filling effects, but starting at different transition densities. Now we examine the role of plasma temperature. In the classical regime, a temperature increase leads to a population shift to high-energy or -momentum states, but low-momentum states are favored for relaxation processes because they transfer momenta more effectively to the phonons. Thus, the rates drop as temperature rises. As for *e-h* scattering, the same argument applies. But since both carrier types are affected by the temperature change, we see an enhancement in its temperature dependence in Fig. 1. As carriers move into the quantum regime, Pauli's principle plays a predominant role in limiting momentum relaxation. Temperature rise however reduces the degree of statistical degeneracy, hence enhances relaxation processes, as demonstrated by the high-density results. At the same time, temperature change also shifts the transition density to a higher value. Finally, difference in the electron and hole masses gives rise to the higher transition density for the latter, as clearly shown by the c–LO-phonon relaxation rates. The higher hole–LO-phonon rate is another manifestation of the larger mass of the holes since it means more effective momentum transfer or relaxation, as more low-momentum states are populated by holes.

It is also interesting to note one consequence of the quantitative difference between the momentum relaxation rates due to c–LO-phonon scattering and the rate due to *e-h* scattering. According to our arguments for the limiting case of strong *e-h* scattering in Ref. [1], the single-component approximation for such a case is marginally justified, as the momentum relaxation rate due to *e-h* scattering (shown in Fig. 1) is only a few times larger than those due to c–LO-phonon scattering around the transparency density.

The Newton type of cooling due to energy exchange between electrons and holes is a pure many-body phenomenon. As far as we know this rate has not been calculated microscopically in the literature. We thus present in the remaining of this section the temperature decay rates due to *e-h* scattering [cf. Eqs. (A13) and (A15) in Ref. [1]] and due to c-LO scatterings [cf. Eq. (B16) in Ref. [1]] in Fig. 2. Qualitatively each decay rate follows similar behavior as its momentum counterpart in Fig. 1 and, thus, only decay rates at 300 K are shown. In addition, the physical understanding is also similar to that for momentum relaxation processes. However, the cooling rates for electrons and holes due to *e-h* scattering are not the same as a result of their different masses. This is in contrast to the situation of momentum relaxation where no such a difference exists. The reason is that the total momentum of the EHP is always conserved so that the momentum relaxation rates have to be the same. However, for temperature cooling it is the total energy that is conserved. Energy conservation only demands that the same amount of energy be exchanged between electrons and holes, but their decay rates also depend on their specific heats. The difference in their specific heats of electrons and holes, owing to their different masses, explains why the cooling rates have to be different for electrons and holes. In the quantum regime, this rate difference is enlarged by the phase-space-filling effects, as seen in the high-density results in Fig. 2. As a result, the holes are much more difficult to cool down than the electrons. Regarding the c-LO cooling rates, we see that holes have a larger rate than electrons as a result of larger population (product of distribution function and the density of states) in the low-energy states. Such lower-energy states are favored for very effective energy transfer to phonons via the scattering, as compared to the lighter electrons. Also, the heavier holes show a higher transition density. Therefore, not only the holes have a larger cooling rate than the electrons, but also a weaker density dependence at the same time.

As we close this section, we note that only momentum relaxation rates are involved in the diffusion coefficients. So, all relaxation rates mentioned below are meant for momen-

tum relaxation unless indicated otherwise.

IV. DIFFUSION COEFFICIENTS FOR A TWO-COMPONENT PLASMA

In this section we present results for the density-related diffusion coefficients in the general two-component case as a function of electron and hole densities, with a constant plasma temperature of 300 K. For convenience, the formulation for the coefficients [1] is collected below:

$$D_{N^eN^e}=\mu_e[(1+\eta_e)S^e_{N^e}+H^h_{N^e}], \tag{5}$$

$$D_{N^eN^h}=\mu_e[(1+\eta_e)H^e_{N^h}+S^h_{N^h}], \tag{6}$$

$$D_{N^hN^e}=\mu_h[(1+\eta_h)H^h_{N^e}+S^e_{N^e}], \tag{7}$$

$$D_{N^hN^h}=\mu_h[(1+\eta_h)S^h_{N^h}+H^e_{N^h}], \tag{8}$$

where $S^\alpha_{N^\alpha}=\partial_{N^\alpha}W^\alpha+N^\alpha\partial_{N^\alpha}\delta\epsilon^\alpha$ and $H^\alpha_{N^\beta}=N^\alpha\partial_{N^\beta}\delta\epsilon^\alpha$ $(\alpha,\beta\in\{e,h\}|\alpha\neq\beta)$. Here $\delta\epsilon^\alpha$ is the many-body correction to the carrier self-energy of type α [cf. Eq. (48) in Ref. [1]]. We refer to $S^\alpha_{N^\alpha}$ and $H^\alpha_{N^\beta}$ as self-terms and mutual terms, respectively, in the ensuing discussions.

A. A few important functions of density and temperature

We note that the DCs in Eqs. (5)–(8) are given in terms of three groups of functions: μ_α's, η_α's, and $\{S^\alpha_{N^\alpha},H^\alpha_{N^\beta}\}$. It helps the interpretation of the results for the coefficients to first analyze these quantities as functions of carrier densities and plasma temperatures. Under the EHP model in the Hartree-Fock framework, all the physical effects can be grouped into free-carrier and many-body contributions. The former includes carrier statistics and c–LO-phonon scattering, while the latter includes many-body corrections to the carrier self-energies and e-h scattering. Note that statistical degeneracy is a kind of carrier correlation and is regarded here as part of free-carrier contributions, since its origin is of statistical nature, rather than the Coulombic carrier-carrier interaction.

We first examine function μ_α, as defined by Eq. (34) in Ref. [1]. Results for the case of equal electron and hole density are shown as an inset in Fig. 1. The main feature of the curves are the linear density dependence at low density, and a generally weak dependence elsewhere. It decreases with temperature at low density, but increases at high density. Obviously, its linear density dependence originates from the secondary density dependence of the e-h scattering rate. This linear density dependence results in a similar secondary density dependence at low density for mutual-diffusion coefficients, as shown later.

Next, we take a close look at function η_α, which is given by $\gamma^\beta_{LO}(m_e+m_h)/\gamma^\beta_{eh}m_\alpha$, essentially the ratio of the c–LO-phonon scattering rate to that of e-h scattering. This function, as can be inferred from Fig. 1, has an inverse linear relationship with the primary density N^α, but is independent of the secondary density N^β at low density. The relationship is weaker than, but close to, linear on both densities at high density. In particular, it has a V-shaped minimum near the transitional primary density, as seen by inverting the Λ shape of the e-h scattering curve in Fig. 1. Its consequent effects on the self-diffusion coefficients will be identified in more detail in the following section. But a qualitative examination of Eqs. (5)–(8) allows us to anticipate the main feature. The magnitude of η_α is of the order of several hundreds at low density and on the order of one near the transition density. So it acts as a magnification factor for the originally weak many-body corrections. In addition, η_e is an order of magnitude larger than η_h because of both the lighter mass of electrons and larger h–LO-phonon scattering rate. Both functions μ_α and η_α produce most of the density dependence for all the coefficients at low density, and further lead to superlinear behavior of the coefficients at high density by adding to the linear dependence from the free-carrier contributions. However, the product of these two functions yields no density dependence at low density. We note that this product is related to carrier mobilities.

The last group of functions are $S^\alpha_{N^\alpha}$ and $H^\beta_{N^\alpha}$. $S^\alpha_{N^\alpha}$'s are normally orders of magnitude greater than $H^\beta_{N^\alpha}$'s, but the margin can be greatly reduced near the transition density. In the extreme case, the margin is merely 50% at the hole transition density when the electron density is high enough. We elaborate and explain the physics underlying the numbers next. The self-terms contain a dominant free-carrier part $(\partial_{N^\alpha}W^\alpha)$ and a negative band-gap renormalization (BGR) part $(N^\alpha\partial_{N^\alpha}\delta\epsilon^\alpha)$, while the mutual terms consist only of a BGR part $(N^\alpha\partial_{N^\beta}\delta\epsilon^\alpha)$. As the free-carrier part has been fully accounted for in Sec. II, we focus upon the BGR parts here. Due to the attractive nature of the Coulomb interaction between electrons and holes, the BGR self-energy itself is negative. The BGR self-energy depends upon the density and temperature through carrier distribution and screening effect. Both the screening effect and the BGR parts diminish at low density, while the former increases with both electron and hole densities in the density range studied in this work. Even though the hole's self-energy contains an additional term [the Coulomb hole (CH) term in Eq. (48) in Ref. [1]], the electron's BGR part in the self-terms behaves similarly as their hole counterpart. Specifically, the part is negative and increases with the primary density but decreases with the secondary density in the density range studied. In contrast, the situation is markedly different for the mutual terms which exist thanks to the screening effect by the secondary carriers. It turns out that the presence of the large CH term in the hole's self-energy dictates that, below the hole transition density, the hole mutual term $H^h_{N^e}=N^h\partial_{N^e}\delta\epsilon^h$ be negative, and the electron mutual term $H^e_{N^h}$ be positive by noting that screening affects the exchange and CH terms oppositely in Eq. (48) in Ref. [1]. The consequence of this difference is, as will be shown in the following sections, that $H^e_{N^h}$ has an appreciable impact on the hole-density coefficients $D_{N^eN^h}$ and $D_{N^hN^h}$, as compared to the negligible role played by $H^h_{N^e}$ on the electron-density coefficients $D_{N^eN^e}$ and $D_{N^hN^e}$. The physical reasons are manifold: First and foremost, the free-carrier part $\partial_{N^\alpha}W^\alpha$ plays a dominant role at lower density for

electrons owing to their lower transition density than for holes. Second, the BGR contributions to the electron-density coefficients are either smaller than their counterparts to the hole-density coefficients or overwhelmed by the free-carrier part because of the first reason. Last but not the least, the order-of-magnitude larger magnification function η_e takes effect.

Concerning the density and temperature dependence of the self-terms and mutual terms, we separately consider the free-carrier and BGR contributions. The free-carrier part relies only on the primary density and temperature. It is density independent and linearly proportional to the temperature in the classical regime. Furthermore, it depends linearly on density and temperature in the quantum regime. The BGR part partially cancels the free-carrier part near the transition density in the self-terms. It increases in magnitude with its primary density, but decreases with the secondary density due to the screening effect. However, the mutual terms are different for electrons and holes. $N^h\partial_{N^e}\delta\epsilon^h$ increases with electron density and decreases with hole density because of screening. By comparison $N^e\partial_{N^h}\delta\epsilon^e$ is negative and decreases in magnitude with electron density due to screening. At the same time it increases in magnitude with hole density when electron density is relatively high, but starts to decrease when the hole density is high enough because of the combined effects of the screening and the CH term. As for the influence of the self-terms and mutual terms on the coefficients, because of the large CH term, the hole-related BGR part in the self-terms has a much larger impact than the electron-related part. Thus, many-body corrections influence the hole-density coefficients much more than the electron-density coefficients.

In connection with the detailed analysis of these important functions above, we conclude this section with a summary of their behavior and their effects on that of the diffusion coefficients in the general two-component case, as will be substantiated quantitatively in the following two sections. The self- and mutual-diffusion coefficients are determined mainly by the free-carrier contributions, but with appreciable many-body corrections near the transition density for the hole-density coefficients. Carrier–LO-phonon scattering is dominant at low density, but electron-hole scattering becomes important in determining their density dependence above the electron transition density. As a result, the self-diffusion coefficients are density independent at low density, and become superlinearly dependent on the primary density. The mutual-diffusion coefficients depend linearly on the secondary density at low density. They become strongly dependent on the electron density, but weaker on the hole density than on the electron density above the electron transition density. All the coefficients depend weakly on the secondary density except $D_{N^eN^h}$. Besides, hole-density coefficients are greatly modified around the hole transition density by many-body corrections.

B. Self-diffusion coefficients: $D_{N^eN^e}$ and $D_{N^hN^h}$

Now we are ready for the presentation of the diffusion coefficients in the general two-component case. We show results for plasma temperature of 300 K only. We note that, in general, increase in plasma temperature leads to the enhancement of the diffusive capability of carriers, as will be seen in Sec. V from the results in the single-component case.

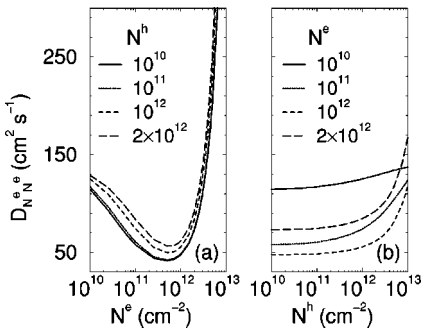

FIG. 3. General two-component electron-hole plasma case: self-diffusion electron-density coefficient $D_{N^eN^e}$ [cf. Eq. (5)] versus electron density (panel a) and hole density (panel b). All data shown in Figs. 3 and 4 are at 300 K including many-body corrections.

Depicted in Figs. 3 and 4 are the numerical results for the self-diffusion coefficients $D_{N^\alpha N^\alpha}$ with $\alpha=e$ and h, respectively. Panel (a) and panel (b) show the dependence of the coefficients on electron and hole densities, respectively. At low density, the coefficients decrease sublinearly with the primary density [Figs. 3(a) and 4(b)], but grow very slowly with the secondary density [Figs. 3(b) and 4(a)]. The dependence on the primary density, however, becomes positive and superlinear at high density. Though the dependence on the secondary density increases, it is weaker than the primary density dependence above the transitional primary density. Near the transition density, the coefficients decrease by as much as 50%, thus forming the valley structures in Figs. 3(a) and 4(b). The overall behavior is comprehensible by recalling our discussions of the important functions in the preceding section. Density independence in the classical regime is expected because the free-carrier part is dominant and independent of density. In addition, function η_α is of the order of several hundreds and its density dependence cancels that of μ_α when the two are multiplied. Carrier diffusion in this regime is dominated by the c–LO-phonon scattering processes, no dependence on either carrier density should be expected as a result. This expectation, however, comes true

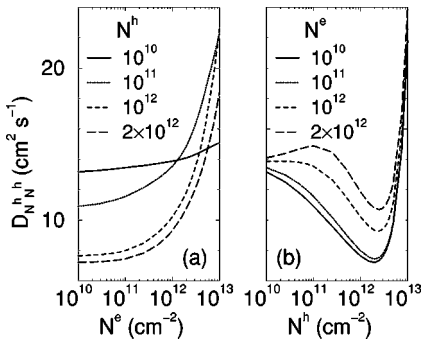

FIG. 4. General two-component electron-hole plasma case: self-diffusion hole-density coefficient $D_{N^hN^h}$ [cf. Eq. (8)] versus electron density [panel (a)] and hole density [panel (b)].

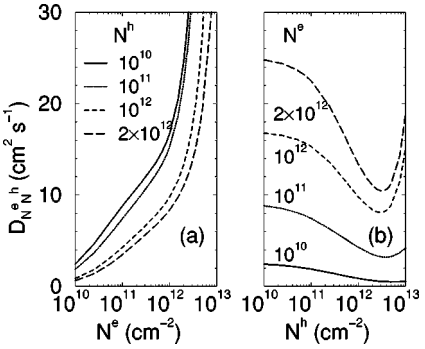

FIG. 5. General two-component electron-hole plasma case: mutual-diffusion hole-density coefficient $D_{N^eN^h}$ [cf. Eq. (6)] versus electron density [panel (a)] and hole density [panel (b)].

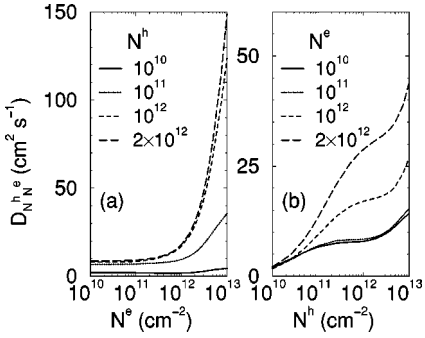

FIG. 6. General two-component electron-hole plasma case: mutual-diffusion electron-density coefficient $D_{N^hN^e}$ [cf. Eq. (7)] versus electron density [panel (a)] and hole density [panel (b)].

only at very low density and could not explain the valley structures shown in Figs. 3 and 4.

The valley stuctures shown in these figures are an indication that the simple Fermi gas picture either in the classical or degenerate limit is not enough to explain the behaviors of the diffusion coefficients. There are two reasons: First, a large density range around the transition density in these figures falls in the intermediate regime between the two extreme limits. Second, many-body effects become important in this range. As seen in the inset of Fig. 1, function μ_α starts to deviate from the familiar linear density dependence of the ideal classical gas behavior at a density of about 5×10^{10} and the dependence becomes much weaker thereafter. At the same time, other factors also start to show deviation from their ideal classical behaviors. For instance, the *e-h* scattering rate at 300 K is 34% lower than its expected value from a linear dependence at the density of 10^{11} cm^{-2}, as shown in Fig. 1. Therefore, the phase-space-filling effects become appreciable before the transition density is reached. Owing to the smaller mass of electrons, such deviations appear at lower density for them than for holes, and in larger magnitude as well. In addition, many-body effects also affect the behaviors of the coefficients, especially around the transition density. In fact, not only the BGR terms become important as carrier density increases, but also *e-h* scattering introduces density dependence through functions μ_α and η_α. As discussed above, the negative BGR part in the self-terms, i.e., $H^\alpha_{N^\alpha}$, partially cancels the free-carrier part, and thus suppresses diffusive processes. As mentioned earlier, many-body effects in this paper contain two parts: the BGR part and the *e-h* scattering. It is interesting to see how each part plays different roles in forming the valley structure in the two self-diffusion coefficients. A direct comparison of the coefficients with and without the BGR contributions reveals that the valley structure for $D_{N^hN^h}$ is mainly due to the BGR contribution from the self-term, but it is the *e-h* scattering that causes the similar structure in $D_{N^eN^e}$. This means that suppression of carrier diffusion can be due to either the attractive Coulomb interaction such that carriers tend to cluster rather than disperse apart, or the increase in the *e-h* scattering rate so that carriers spend more time bouncing around locally rather than wandering away. The more frequent collisions for holes with LO phonons at low density mean less diffusive capability or a smaller DC for them. Consequently, *e-h* scattering influences the diffusive capability of electrons more than that of holes. Therefore, the reduction in the diffusive capability of electrons is mainly due to the enhancement of *e-h* scattering as carrier density increases, and BGR contribution is responsible for such suppression in the diffusivity of holes.

It is relatively straightforward to understand the results at high density. Free-carrier contributions to the self-terms have a linear primary density dependence and no dependence on the secondary density. Additionally, they are predominant over the BGR parts. As a result of the combined effects of functions μ_α, η_α, and the self-terms, the coefficients increase superlinearly with the primary carrier density [cf. Figs. 3(a) and 4(b)], but more weakly with the secondary carrier density [cf. Figs. 3(b) and 4(a)].

C. Mutual-diffusion coefficients: $D_{N^eN^h}$ and $D_{N^hN^e}$

The mutual-diffusion coefficients $D_{N^\alpha N^\beta}$ with α, $\beta \in \{e,h\} | \alpha \neq \beta$ are shown in Figs. 5 and 6, respectively. Panels (a) and (b) depict the dependence of the coefficients on electron and hole densities, respectively. The coefficients decrease and go to zero following the secondary density. They are independent of the primary density at low density [Figs. 5(b) and 6(a)]. At high density, they feature a superlinear growth with the electron density, but a much weaker one with the hole density. For $D_{N^eN^h}$, a similar valley structure appears for high electron densities [Fig. 5(b)], but the bottom of the valley appears at a higher density than for $D_{N^hN^h}$ [Fig. 4(b)] around the hole transition density. For $D_{N^hN^e}$, however, no appreciable feature shows up around the electron transition density [Fig. 6(a)], as compared to $D_{N^eN^e}$ [Fig. 3(a)]. Finally, on secondary density dependence, a more pronounced slowdown of the transitional growth in the coefficients is observed for $D_{N^hN^e}$ near the hole transition density in Fig. 6(b) than for $D_{N^eN^h}$ near the electron transition density in Fig. 5(a).

These behaviors can be understood similarly as for the self-diffusion coefficients in terms of the several functions discussed in Sec. IV A [cf. Eqs. (5)–(8)]. We start with low-density results. In this classical regime, the free-carrier contributions have no density dependence and the BGR terms diminish so that the coefficients are well described by $D_{N^\alpha N^\beta} \approx \mu_\alpha S^\beta_{N^\beta}$. As such, the coefficients inherit the second-

ary density dependence of function μ_α, or a linear dependence (Fig. 1 inset). The coefficients have no dependence on the primary density either. Nevertheless, deviations exist due to exactly the same reasons discussed in the preceding section. After comparing with results without BGR contributions (not shown), it is found that the mutual term $H^e_{N^h}$ approximately doubles $D_{N^eN^h}$ when the electron density is above its transition density [Fig. 5(b)]. The enhancement is attributed to function η_e whose value is about 400 at 10^{10} cm^{-2}—that is why we call it a magnification factor. Physically, it is easy to understand these behaviors of the coefficients. The mutual-diffusion process is a consequence of interaction between carriers. The interaction results in both many-body corrections to the self-energy of carriers and incoherent scattering events (higher-order correlation) between them. It is trivially expected that the effects of the interaction on carriers of the secondary type vanish if secondary density becomes too small in the EHP model [8]. This induced diffusive process is elevated as secondary density increases, though increase in primary density impedes such an enhancement by introducing stronger scattering and more negative many-body corrections. As carrier densities are near their transition densities, quantitative differences in the functions discussed in Sec. IV A between electrons and holes take effect. As a result, many-body corrections have a much more noticeable impact on $D_{N^eN^h}$ than on $D_{N^hN^e}$. One indication is in Fig. 5(b), where the hole-density dependence features a remarkable dip near the transition density for $D_{N^eN^h}$. This behavior is because the positive BGR contribution to the mutual term doubles the coefficients at low density through the magnification factor, in conjunction with a partial cancellation of the free-carrier contribution by the negative BGR part in the self-term [cf. Eq. (6)]. The cancellation is most pronounced near the transition density. For $D_{N^hN^e}$ [cf. Eq. (7)], the free-electron contribution overwhelms the BGR term in the self-term, whereas the larger but negative BGR contribution in the mutual term is partially offset by the order-of-magnitude smaller magnification factor η_h. As a matter of fact, function η_h takes a value of 1 as compared to a value of 10 for η_e when both electron and hole density are 10^{12} cm^{-2}. As such, the many-body corrections bring about the valley structure in $D_{N^eN^h}$. However, many-body corrections do cause a more distinguishable slowdown in its transition into the quantum regime for $D_{N^hN^e}$ near the hole transition density, as shown in Fig. 6(b). Finally, above the transition densities, free-carrier contributions take over and superlinear growth takes hold for the coefficients. In comparison with the self-diffusion coefficients, the density dependence of the mutual-diffusion coefficients is much weaker because of the displacement of the magnification factor η_α from the self-terms to the mutual terms [cf. Eqs. (5)–(8)].

In summary, mutual-diffusion coefficients describe the induced diffusive capability of the secondary carriers by interacting with the primary carriers. As a result, the coefficients go to zero with the secondary densities. In addition, many-body corrections have more pronounced effects in these coefficients, especially in $D_{N^eN^h}$.

V. THE AMBIPOLAR DIFFUSION COEFFICIENTS

In this section, we present numerical results for all four ambipolar diffusion coefficients and analyze their dependence on plasma density and temperature, as well as the effects of many-body corrections. For convenience, we choose the word ''ambipolar'' to represent the results for the single-component case without further implication. Under the single-component approximation, the EHP is neutral and all its thermodynamic properties are characterized by the plasma density and temperature. For easy reference and discussions, the expressions for the coefficients are rewritten below:

$$D_{NN}=\mu(\partial_N W+N\partial_N\delta\epsilon_g), \tag{9}$$

$$D_{NT}=\mu(\partial_T W+N\partial_T\delta\epsilon_g), \tag{10}$$

$$D_{TN}=[2j_W(W/N)-j_N]D_{NN}, \tag{11}$$

$$D_{TT}=[2j_W(W/N)-j_N]D_{NT}, \tag{12}$$

where W is the total thermal energy of the EHP and $\delta\epsilon_g=\delta\epsilon^e+\delta\epsilon^h$ is the total BGR energy. Furthermore, we have

$$\mu=1/(m_e\gamma^e_{\rm LO}+m_h\gamma^h_{\rm LO}), \tag{13}$$

where j_W and j_N are transformation Jacobians [1]. We point out that the *e*-*h* scattering rate drops out in the present case. The absence of the effects of *e*-*h* scattering in the ambipolar mobility was noted in Ref. [9]. Similarly all the ambipolar diffusion coefficients are independent of the scattering. Similar to the general two-component case, we start by analyzing the contributing factors to the DCs in terms of their dependence on the thermodynamic variables of the EHP, followed by a presentation of the results for the DCs and the associated many-body effects.

A. Density and temperature dependence of the contributing factors

As shown in Eqs. (9)–(12), there are four contributions to the diffusion coefficients: (1) incoherent scattering by factor μ, (2) free-carrier part represented by the derivatives of the total thermal energy W, (3) coherent many-body part represented by the derivatives of the BGR $\delta\epsilon_g$, and (4) the prefactor in the expressions of D_{TN} and D_{TT} in Eqs. (11) and (12). The first three contributions have been elaborated somewhat in the two-component case in Sec. IV A. In the following, we point out their ramifications in the single-component case and focus on the BGR contributions instead. A summary of the many-body effects is published elsewhere [10].

To begin with, we note that the factor μ [cf. Eq. (13)] is independent of plasma density in the classical regime, and has a sublinear density dependence above the hole transition density owing to the dominance of the h–LO-phonon scattering rate. The factor increases weakly with plasma temperature in the classical regime, and becomes even more insensitive to temperature in the quantum regime thanks to the mixed contributions from the c–LO-phonon scattering rates.

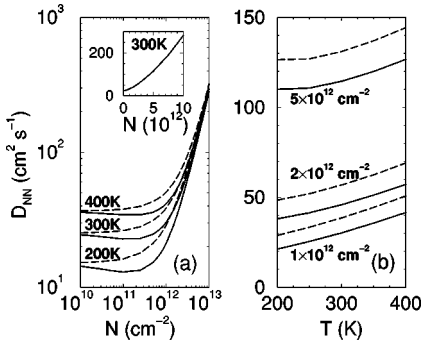

FIG. 7. The electron-hole plasma under single-component approximation case: self-diffusion density coefficient D_{NN} [cf. Eq. (9)] versus plasma density [panel (a)] and temperature [panel (b)]. Solid lines include many-body corrections to the free-carrier results (dashed lines), and the same notation is also used in Figs. 8–10. The inset shows the 300-K data with many-body effects in linear *X*-*Y* scale.

Second, the free-carrier part, as in the two-component case, dominates over the BGR part. In the classical regime, the free-carrier contribution yields no density and linear temperature dependence for density diffusion coefficients, and no temperature but linear density dependence for temperature diffusion coefficients. In the quantum regime, it gives rise to a linear density and no temperature dependence for density diffusion coefficients, and linear temperature but no density dependence for temperature diffusion coefficients. Furthermore, the density derivative of the thermal energy $\partial_N W$ displays the transition density of the electrons, in contrast to the temperature derivative of the thermal energy $\partial_T W$, which shows that of the heavier holes when the EHP transits from the classical to quantum regime. As explained in Sec. IV A, lighter electrons enter the quantum regime at a lower density than holes. In the quantum regime, the contribution to the total thermal energy from electrons is enhanced because the energy of electrons now increases faster with density. However, the enhanced contribution has a weaker temperature dependence. With all factors in, free-carrier contributions show different transition densities in density and temperature diffusion coefficients. Third, we discuss the BGR parts in Eqs. (9)–(12). In comparison with the general two-component case, the *e*-*h* scattering rate and mutual terms drop out. The BGR parts in the self-terms are the only remaining many-body contributions. Therefore, in general, many-body effects have a less drastic impact in the ambipolar case as a result of the missing contributions and the dominant free-carrier contribution from electrons. Since the BGR energy is negative and increases in magnitude with carrier density [11–13], its derivative with respect to density, $N\partial_N \delta\epsilon_g$ as appeared in Eqs. (9) and (11), is negative. The magnitude of the BGR term grows with density and tends to saturate at high density. But the term is insensitive to temperature. On the other hand, because the increase in temperature reduces the magnitude of the BGR [14], the temperature derivative $N\partial_T \delta\epsilon_g$ is positive. The magnitude of the term increases superlinearly with density at low density and tends to saturate at high density. This term is also insensitive to temperature. Overall, the many-body effects are relatively weakened by temperature, since the free-carrier contributions become more influential with an increase in temperature. Finally, the prefactor $2j_W(W/N)-j_N$ turns out to follow approximately an inversely linear dependence on the density and increase with plasma temperature in the whole covered range, which can be easily verified by recalling that the Jacobians are defined by $j_W=1/\partial_T W$ and $j_N=\partial_N W/\partial_T W$ and using Eq. (1).

B. Self-diffusion density coefficient: D_{NN}

Figure 7 shows the self-diffusion coefficient D_{NN} as a function of plasma density (a) and temperature (b). Solid and dashed curves in the figures represent results with and without the BGR terms, respectively. The self-diffusion density coefficient D_{NN} displays a superlinear density dependence at high density, and is almost constant at low density. The transition in the density dependence occurs at the electron transition density and shifts toward higher density with temperature. The temperature dependence is linear at low density, but somewhat nonlinear at high density as shown in Fig. 7(b). These behaviors are mainly attributed to the free-carrier part $\partial_N W$ in Eq. (9). As discussed earlier, factor μ is essentially density insensitive in the whole covered range. The BGR term brings some correction to the free-carrier term, but does not change the basic behavior of the coefficient, as discussed next. It is the free-carrier part that is responsible for the basic behavior of the coefficient. In particular, the dominant part increases from the classical value of $2k_BT$ to a value of the order of the chemical potential for electrons as the EHP transits from the classical into the quantum regime. Thus, the coefficient D_{NN} has no density dependence and linear temperature dependence at low density. In the intermediate density range, as the lighter electrons lead holes in the transition, the transition density in Fig. 7(a) coincides with the electron transition density, and it increases with temperature, as indicated in Eq. (3). In the quantum regime, the chemical potential for electrons is approximately given by $\pi\hbar^2 N/m_e$. Therefore, these properties of the free-carrier part, together with factor μ, produce the superlinear density dependence and nonlinear temperature dependence of D_{NN} at high density. We remark that the drastic increase in the coefficient near the transition density is not mainly due to the weakening in scattering. As noted, factor μ solely conveys the effects of scattering. It is clearly shown in Eq. (13) and Fig. 1 that the h–LO-phonon scattering plays a dominant role. Since the scattering is basically density independent in the covered range, we conclude that scattering is not responsible for the observed strong enhancement at high density. Instead, the enhancement comes directly from a density-dependent gain in the thermal energy of the EHP as a result of the statistical transition. As a matter of fact, such a gain appears as a prefactor in Landsberg's generalized Einstein relation [15]. Lastly, we note that in the classical regime, the Einstein relation is recovered as $D_{NN}=2k_BT\mu$. Interestingly, in the quantum regime the relation is modified not only by the enhancement due to the energy gain, but also by the many-body corrections.

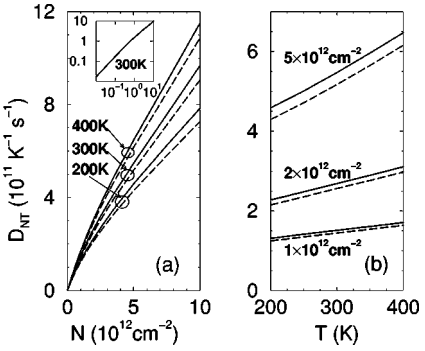

FIG. 8. The electron-hole plasma under single-component approximation case: mutual-diffusion temperature coefficient D_{NT} [cf. Eq. (10)] versus plasma density (a) and temperature (b). Linear *X*-*Y* scale is used in order to show the weak temperature dependence. The inset shows the 300-K data in a log-log scale for comparison.

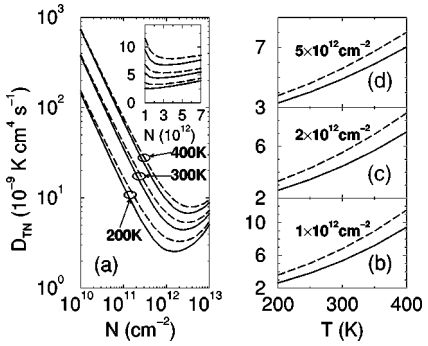

FIG. 9. The electron-hole plasma under single-component approximation case: mutual-diffusion density coefficient D_{TN} [cf. Eq. (11)] versus plasma density (a) and temperature (b)–(d). The inset shows the same data in linear *X*-*Y* scale for comparison. Multiple panels (b)–(d) are used to better illustrate the temperature dependence of the coefficient, as in Fig. 10.

Next, we discuss many-body effects on the coefficient D_{NN}. The effects stem from the BGR term $N\partial_N\delta\epsilon_g$ in Eq. (9). They result in the difference in Fig. 7 between the solid curves (with BGR term) and the dashed curves (without BGR term). The BGR contribution increases in size with density at low density and reaches a maximum near the electron transition density, then decreases at high density. Temperature has no appreciable effect on the BGR contribution as best seen in panel (b), which is in the linear *X*-*Y* scale. The reduction in the coefficient by many-body effects is expected because of the attractive nature of Coulomb interaction between electrons and holes. Thus, their diffusivity or diffusion coefficient is reduced as compared to the interaction-free case. Further reduction results as interaction intensifies with density. On the contrary, increase in plasma temperature enhances the thermal motion of the EHP so that the significance of the interaction is relatively weakened. The reduction introduced by many-body effects can be over 20% [10].

C. Mutual-diffusion temperature coefficient: D_{NT}

The results for the mutual-diffusion temperature coefficient D_{NT} are shown in Fig. 8 in linear *X*-*Y* scale in the main panels (a) for density dependence and (b) for temperature dependence. Additionally, the 300-K data with BGR contribution are plotted in log-log scale as an inset for comparison. At low density, the coefficient depends on the density linearly but not on the temperature. At high density, its density dependence is sublinear [Fig. 8(a)], while the temperature dependence is linear [Fig. 8(b)]. It is noted from panel (a) and the inset that the statistical transition is characterized by the hole transition density. In the classical regime, the linear density-dependent and temperature-independent behavior is expected because the dominant free-carrier term dictates such a behavior with factor μ having no density and weak temperature dependence. In the quantum regime, the dominating free-carrier part produces a linear temperature dependence but no density dependence. The sublinear density dependence comes from factor μ, as discussed in Sec. V A. Recall that both the free-carrier part $\partial_T W$ and factor μ follow the hole transition density as they enter the quantum regime, which account for the observed transitional behavior. The overall behavior of the coefficient fits perfectly to our general understanding of the physics involved. First of all, due to its induced nature, mutual diffusion is expected to vanish with the secondary variable. The linear density dependence at low density manifests the consistency. Second, as carriers become statistically degenerate, the induced current is reduced by the phase-space-filling effects. In the quantum regime, thermal excitation of carriers is restrictive as compared to the classical case, which leads to smaller diffusivity. Temperature elevation tends to lift the restriction, thus we see an increase in the coefficient (cf. Fig. 8).

Many-body effects on coefficient D_{NT} are shown by the difference between the solid and dashed curves in Fig. 8. As seen, many-body effects increase the diffusion coefficient, and the increase grows with density in the range shown. The effects are temperature independent, however. Comparatively, the many-body effects on D_{NT} are weaker than on D_{NN}. From Eq. (10), the coefficient is influenced by many-body effects through the BGR term $N\partial_T\delta\epsilon_g$, which is positive in the studied range (cf. Sec. V A and Ref. [14]). Also, the BGR term increases superlinearly with density and depends weakly on temperature. In addition, factor μ shows both weak density and temperature dependence. Thus, the many-body effects behave as numerically expected. Physically, the effects are understood as follows: Recall that D_{NT} represents a measure of efficiency for the induced contribution from a temperature gradient to density current. The induced current would flow from the high-temperature region to the low-temperature region as many-body effects increase the diffusion coefficient. As the negative BGR self-energy is lower in the low-temperature region [14], force is thus induced by the temperature gradient and helps current flow. Therefore, the induced current does flow in the right direction, so many-body effects contribute positively to the coefficient. Finally, it is worth noting that, as indicated by Eqs. (9)–(12), the two remaining DCs are affected by many-body effects in the same manner as the two we just showed, so the effects shall not be further discussed.

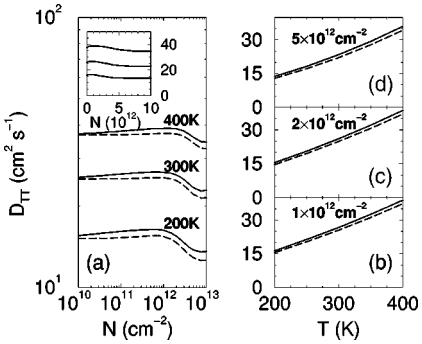

FIG. 10. The electron-hole plasma under single-component approximation case: self-diffusion temperature coefficient D_{TT} [cf. Eq. (12)] versus plasma density (a) and temperature (b). The inset shows the many-body corrections-included data in linear *X*-*Y* scale for comparison.

In summary, many-body effects reduce the density coefficients but enhance temperature coefficients. Plasma temperature has negligible influence over the effects on all the coefficients.

D. Mutual-diffusion density coefficient: D_{TN}

In this section, we present the results for the mutual-diffusion density coefficient D_{TN} in Fig. 9. Density and temperature dependence of the coefficient are plotted in panels (a) and (b)–(d), respectively. In the inset of panel (a), the same data are presented in the linear *X*-*Y* scale for comparison.

As seen, the coefficient decreases linearly at low density and increases sublinearly at high density. The transition occurs at a higher density than for D_{NN} and seemingly follows the hole transition density. The temperature dependence shows stronger than linear behavior. Understanding these results is straightforward by examining Eq. (11) and recalling the behavior of the prefactor (see Sec. V A). The prefactor $2j_W(W/N)-j_N$ depends inversely on density but linearly on temperature, which translates into an inverse proportionality of the coefficient to density at low density and sublinear dependence at high density. Furthermore, the prefactor masks the electron transition density by shifting the transition density to a higher value than for D_{NN}, and further transforms the high-density behavior of D_{TN} from the superlinear dependence of D_{NN} to the present sublinear dependence in Fig. 9(a). On the other hand, the temperature dependence of D_{TN}, as seen in Figs. 9(b)–9(d), becomes stronger than that of D_{NN}, as enhanced by the prefactor. Now we examine the results from the physical perspective. The present coefficient measures the temperature diffusivity induced by a density gradient. First, it vanishes with the secondary variable, i.e., plasma temperature, at low temperature, as expected and indicated in Figs. 9(b)–9(d). Second, at low density, thermal energy current flows in proportion with density gradient as the energy scales linearly with density. However, temperature, as an intensive quantity, does not scale with density. Thus, the induced temperature diffusivity scales inversely with density. As phase-space-filling effects set in when density increases, the diffusivity is enhanced because of increase in the energy at the same temperature as compared to the classical case, as revealed in panel (a). Then temperature elevation increases the energy at any given density, which improves the mutual diffusion in the whole range shown.

E. Self-diffusion temperature coefficient: D_{TT}

We present the results for the self-diffusion temperature coefficient D_{TT} in this section in the same manner used for D_{TN}. As shown in Fig. 10, the coefficient shows a positive but quite weak dependence on density at low density and a sublinear decrease above the hole transition density. A slightly superlinear temperature dependence is shown by the coefficient. Similar to D_{TN}, the behavior of the coefficient can be numerically understood starting from the prefactor and D_{NT} [see Eq. (12)]. Therefore, we shall omit discussions from the numerical viewpoint. Instead we focus on the physical interpretation of the results. To start with, we note that the self-diffusion of temperature is associated with the thermal energy of the carriers. This is the fundamental reason why the two self-diffusion coefficients D_{NN} and D_{TT} share similar values in the classical regime, as shown in Figs. 7 and 10. The thermal energy is linearly proportional to density and temperature at low density, which lead to the well-known Wiedemann-Franz law [3]. Hence the self-temperature-diffusion correlates with self-density-diffusion, which results in quantitatively similar behaviors between the two self-diffusion coefficients. However, in the quantum regime, statistical degeneracy completely breaks down the bilinear dependence of the energy on density and temperature. The self-diffusion density coefficient is drastically enhanced because of the phase-space-filling effects (see Sec. V B). The enhancement is associated with both increased thermal energy and reduced scattering rates (see Fig. 1). But the increase in thermal energy has been shown to be mainly caused by the quadratic density term $w_0^{\alpha}N^{\alpha 2}$ in Eq. (1). Simultaneously, temperature-dependent terms in the quantum regime are greatly reduced in magnitude. As such, the increase in thermal energy has an adverse effect on D_{TT}. Similarly, the reduction in scattering rates does not help the self-diffusion temperature coefficient. Rather, less scattering means less thermal motion as if the temperature were lower. Therefore, we see how physically the coefficient decreases with density in the quantum regime. The effect of temperature elevation is comprehensible in a similar manner to the other coefficients discussed earlier, and thus shall not be repeated.

In summary, it has been shown for the diffusion coefficients under the single-component approximation that many-body effects suppress the density coefficients, but enhance the temperature coefficients. The modification is on the order of 10% and can reach over 20% [10] for the density coefficients. The effects increase with density for the temperature coefficients within the range studied. However, many-body effects play a minor role in determining the dependence of the coefficients on plasma density and temperature. Free-carrier contributions are dominantly responsible for such dependence. In the classical regime, self-diffusion coefficients have a negligible density dependence. In the quantum re-

gime, however, the density coefficient D_{NN} is enhanced to a superlinear dependence, whereas the temperature coefficient D_{TT} is reduced sublinearly, as a result of statistical degeneracy. By contrast, mutual-diffusion coefficients behave distinctly differently. The temperature coefficient D_{NT} vanishes linearly with the density in the classical regime, but the density coefficient D_{TN} scales inversely with density. In the quantum regime, both of them scale sublinearly with density. Overall, temperature elevation enhances all the diffusion coefficients linearly, and the enhancement increases with density.

VI. SUMMARY AND CONCLUDING REMARKS

In this section, we make a few general comments on certain aspects of our coupled diffusion model and the numerical results presented in the previous sections. By doing so, we shall achieve a deeper physical understanding of the present hydrodynamic description of transport in the EHP in a quasi-two-dimensional QW structure.

First of all, it is realized that a general treatment of carrier transport at low density on the hydrodynamic level is hindered by a Coulomb interaction of carriers. Sophisticated theoretical work exists on such exciton-plasma systems for moderately low-density and pure excitonic systems at lower density [16,17], but state-of-the-art laser models fail to include such complexity. In this regard, the CDM represents an effort towards incorporating such physical complexity. This is the premise upon which we justify our low-density results. As such, we call the low-density range below the transition densities the classical regime. Furthermore, this choice of terminology also implies a classical statistical treatment and an extension of many-body theoretical results, which includes the BGR contributions and scattering rates to this regime.

Next, some observations on the many-body effects on the diffusion coefficients are in order. As shown, the BGR contributions and *e-h* scattering play drastically different roles in the general TC case than in the SC case. Nevertheless, the results are consistent, as expected, since the single-component case is just a limiting case of the general two-component case. If the electron-hole pair in the EHP is treated as a single entity, as being done under the single-component approximation, the incoherent *e-h* scattering drops out and has no influence on plasma transport. However, the BGR contributions do have an effect on all the DCs, even though the size of the effect varies from coefficient to coefficient.

Now we make a comparison between the self-diffusion density coefficient D_{NN} in our quasi-2D case and its counterpart in the 3D case under the ambipolar diffusion approximation. The coefficient for bulk GaAs was calculated in Ref. [18] (solid curve in the lower panel of Fig. 7 therein) as a function of plasma density. The result is compared to our quasi-2D result in Fig. 9(a). A similar transition of the density dependence from the classical to quantum regime is shown in the 3D case, and our coefficient is marginally larger than the bulk value in the density range shown. The transitional behavior in our quasi-2D case is found to occur at a smaller corresponding density than in the 3D case. To understand this difference, we reiterate that the transition is attributed to the effect of statistical degeneracy. As free fermions become degenerate, their energy scale is the chemical potential instead of the thermal energy k_BT. Needless to say, the classical energy scale is density independent. The chemical potential in the quantum regime is mainly determined by the plasma density, but its value depends on dimensionality because of the different density of states. Therefore, physical quantities of an EHP in different dimensions have different values, such as the transition density under discussion. To make a more specific comparison, we give the transition density $n_{t,\alpha}^{3D}$ in the 3D case below [4]:

$$n_{t,\alpha}^{3D}=2\left(\frac{m_\alpha k_B T}{2\pi\hbar^2}\right)^{3/2}\frac{2}{\sqrt{\pi}}\int_0^\infty d\epsilon\,\frac{\sqrt{\epsilon}}{1+\exp(\epsilon)}. \tag{14}$$

For electrons it is $\approx 10^{18}$ cm^{-3}, and $\approx 10^{19}$ cm^{-3} for holes at room temperature. Thus, the difference in the transition densities is explained in terms of numerics. Next, we further consider this difference from a physical perspective. It is known that reduced dimensionality makes it easier for fermionic particles to feel the presence of each other as compared to higher dimensions for a simple geometric reason. The fermionic gas becomes statistically degenerate when carrier density is high enough or temperature low enough such that particles which are characterized by the de Broglie wavelength overlap with each other. This means that the transition density is smaller than its counterpart in the bulk material and the lighter electrons have a lower transition density than the holes. As such, we explain the shift in the transition densities in the 2D and 3D cases. Other than D_{NN}, transitional behaviors in their density dependence also exist for the other DCs in the quasi-2D case. It would be interesting to compare the quasi-2D results with 3D ones for other diffusion coefficients.

Last but not the least, we comment on the application aspects of the CDM in the general two-component case where spatial charge separation occurs. Such a situation can happen in type-II QWs or by external modulation of the quantum confinement potential. It is interesting to note that even though the screening effect is weakened in such cases, higher mobility could, in principle, be achieved through the reduction of *e-h* scattering due to a reduced spatial overlap between oppositely charged particles. Furthermore, innovative device designs could be conceptualized by the realization of negative mobility for minority carriers under certain conditions.

To conclude, we have presented numerical results for density-related diffusion coefficients in the general two-component case together with results for all the diffusion coefficients in the single-component case for the coupled diffusion model as functions of carrier densities and temperatures of the electron-hole plasma. Also presented are momentum and temperature relaxation rates due to carrier–LO-phonon scattering and electron-hole scattering, which are calculated microscopically and used for the diffusion coefficients. The diffusion coefficients are analyzed in the framework of the free Fermi gas theory with many-body effects

included. Free-carrier contributions derive from carrier thermal energy and carrier–LO-phonon scattering, whereas many-body effects originate from band-gap renormalization and electron-hole scattering. In the general two-component case, appreciable many-body corrections occur near the hole transition density for hole-density coefficients. Carrier–LO-phonon scattering dominates at low density, but electron-hole scattering becomes important in determining the density dependence above the electron transition density for all the coefficients. In the single-component case, many-body effects suppress density coefficients but enhance temperature coefficients. The modification is on the order of 10% and reaches a maximum of over 20% [10] for the density coefficients. The effect increases with density for the temperature coefficients within the range studied. However, the many-body effects play a minor role in determining the dependence of the coefficients on plasma density and temperature, as compared to the two-component case. Overall, temperature elevation enhances the diffusion coefficients linearly, and such an enhancement increases with density. Many-body effects on the coefficients are insensitive to temperature. Simulation results based on the CDM will be presented in a future work. Finally, we point out that the CDM in the general two-component case can be incorporated into design tools for innovative optoelectronic devices.

ACKNOWLEDGMENT

This work was supported in part by the Director's Discretionary Fund of the NASA Ames Research Center.

[1] J. Li and C. Z. Ning, preceding paper, Phys. Rev. A **66**, 023802 (2002).
[2] For the Fermi gas theory, consult any textbooks on solid-state physics, such as Ref. [3]. For many-body corrections, refer to Refs. [6,7,11,16,17].
[3] N. W. Ashcroft and N. D. Mermin, *Solid State Physics* (Holt, Rinehart and Winston, New York, 1976).
[4] H. E. Ruda, J. Appl. Phys. **59**, 1120 (1986).
[5] L. P. Kadanoff and G. Baym, *Quantum Statistical Mechanics* (Addison-Wesley, Reading, MA, 1989).
[6] S. W. Koch and H. Haug, *Theory of the Electrical and Optical Properties of Semiconductors*, 3rd ed. (World Scientific, Singapore, 1994).
[7] W. W. Chow, S. W. Koch, and M. Sargent III, *Semiconductor Laser Physics* (Springer-Verlag, Berlin, 1994).
[8] In our treatment of the Coulomb interaction within the electron-hole plasma model, the singularity in the potential cannot be properly accounted for, which means that no excitonic bound states are recovered, as far as carrier transport properties are concerned. As a result, the low-density limit for many-body contributions is zero.
[9] J. R. Meyer, Phys. Rev. B **21**, 1554 (1980).
[10] C. Z. Ning and J. Li, Phys. Rev. B **65**, 201305(R) (2002).
[11] H. Haug and S. W. Koch, Phys. Rev. A **39**, 1887 (1989).
[12] S. Schmitt-Rink, C. Ell, and H. Haug, Phys. Rev. B **33**, 1183 (1986).
[13] J. Li and C. Z. Ning, Proc. SPIE **3944**, 311 (2000).
[14] R. Zimmermann, Phys. Status Solidi B **146**, 371 (1988).
[15] P. T. Landsberg, Proc. IEEE **61**, 476 (1973).
[16] H. Haug and S. Schmitt-Rink, Prog. Quantum Electron. **9**, 3 (1984).
[17] R. Binder and S. W. Koch, Prog. Quantum Electron. **19**, 307 (1995).
[18] O. Hess and T. Kuhn, Phys. Rev. A **54**, 3347 (1996).
[19] *Numerical Data and Functional Relationships in Science and Technology*, edited by O. Madelung, Landolt-Börnstein, New Series, Group III, Vol. 17B (Springer-Verlag, Berlin, 1987).